Radiochimica Acta 27, 125–130 (1980)

Cross Sections and Thick Target Yields of (d, xn) Reactions on Natural Lead

By C. WASILEVSKY, M. DE LA VEGA VEDOYA and S. J. NASSIFF, Comision Nacional de Energia Atomica
Buenos Aires, Argentina

(Received October 22, 1979; revised March 3, 1980)

Lead/Deuteron reactions/Excitation functions/Isotope production

Abstract

Target foil stacks of lead were bombarded with beams of deuterons at incident energies ≤ 27.5 MeV. Excitation functions for the production of ^{203}Bi, ^{204}Bi, ^{205}Bi, ^{206}Bi, and ^{207}Bi by (d, xn) reactions were determined. On the basis of the cross sections, the thick target yields and saturation production rates of ^{205}Bi, ^{206}Bi and ^{207}Bi have been evaluated.

Introduction

The estimated excitation functions may serve as a basis for technical and economical evaluation of the production of radioisotopes by means of a cyclotron [1–2].

In other way, although measurement of integrated cross sections does not allow a very detailed interpretation of the reaction mechanisms, it is hoped that it will provide a useful background for a further study of these reactions about which so little is known [3–4].

Finally, in view of the current interest in the levels of the element lead found in human tissues, we have reviewed the formation of some of those bismuth and lead isotopes which might fulfil the criteria for usefullness as tracers in vivo [5–8].

Experimental

a) Irradiations

The experiments were performed in a manner similar to that outlined in previous papers [9–13].

Stacks of lead foils (~ 31.2 mg/cm^2) were irradiated in the external beam of the 60 inch Synchrocyclotron. In each case the target stack was thick enough to stop the 27.5 MeV deuteron external beam. Maximum uncertainty in the incident beam energy was estimated as being lower than 1%. The lead foils were analyzed spectroscopically for interfering impurities; the amounts of these were found to be negligible.

Within the stacks, used for the determination of excitation functions and thick target yields, aluminium foils were inserted. The Al foils were used to degrade the energy of the deuterons and also for the determination of the excitation function of the reaction ^{27}Al (d, αp) ^{24}Na, used to monitor the ion current. The excitation functions values established by MARTENS and SCHWEIMER [14] were taken as standard.

The mean deuteron energy for each foil was calculated by means of a computer program based on the range energy relationships given in the literature [15].

The uncertainty in the incident particle energy for each data point arises from the energy spread of the incident deuteron beam as well as from the energy straggling losses. The latter was estimated to be about 0.5 MeV for the foil in which the deuterons had been slowed down to 16 MeV [16].

b) Counting

Production cross sections were measured by a nondestructive determination of the activation products. After bombardment, gamma photons were detected with a semiconductor coaxial Ge(Li) detector in connection with a multichannel pulse height analyser.

Enough data was taken at time intervals suitable for nuclide identification. A check of half-life and gamma ray energies was carried out.

Standard sources of gamma emitters with well known values of energy and intensities of gamma rays were used for an accurate calibration of the energy and detection efficiency of the spectrometer. Most efficiency determinations agreed within the statistical error of 3%.

Efficiency $E\,(E_\gamma)$ was calculated for other energies using:

$$(E_\gamma) = C \cdot E_\gamma^{-n}.$$

Using WASSON's method, the respective values of counts per unit time were computed after the recording of each photopeak [17–18].

The areas of all gamma peaks observed were corrected for efficiency of detection and the activities of the radioactive products were calculated separately for each peak on the basis of the nuclear data [19–20].

No corrections were made either for the energy spread at each foil (as resulting from foil thickness variations) or for energy losses at the preceding foils. The eventual losses of reaction products by recoil were assumed to be negligible. As for any reactions that might occur due to secondary neutrons, additional foils were set up beyond the range of deuterons. Spectra from those foils showed no significant contribution to our data.

Uncertainties in the cross section values were estimated by propagating in quadrature the contributions from both decay curve and peak analyses (the latter including counting statistics), absolute detector efficiencies, disintegration schemes, target thicknesses and deuteron flux.

Results and conclusions

Fig. 1 and Table 1 display the ^{204}Pb (d, 3n) ^{203}Bi excitation function. Due to the small isotopic abundance of

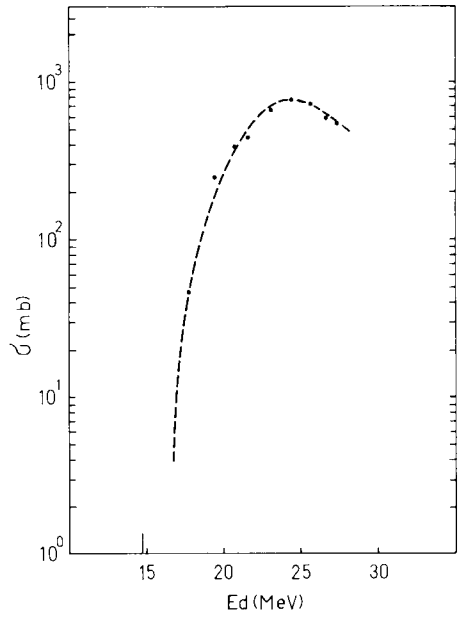

Fig. 1. Absolute cross sections for ^{204}Pd (d, 3n) ^{203}Bi reaction

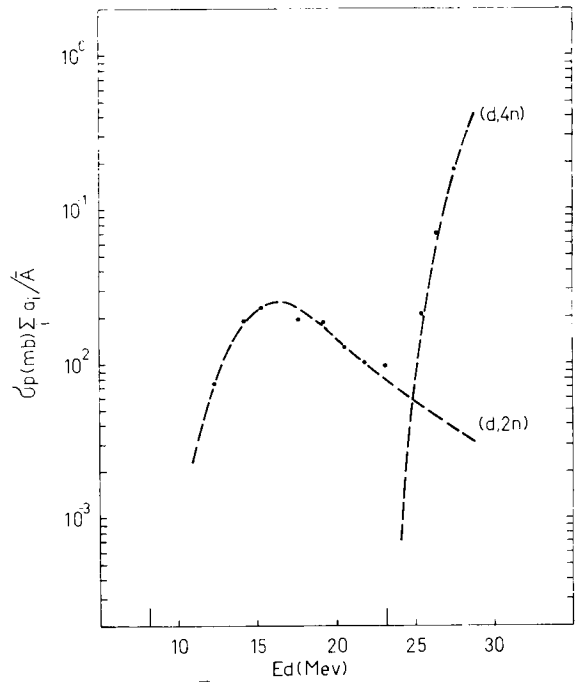

Fig. 2. $\sigma_p(\text{mb})\sum_i a_i/\bar{A}$ for ^{204}Bi. Dashed lines represent the estimates of different possible reactions

^{204}Pb the cross sections have been determined with a large error.

In some cases, different reactions contribute to form the same nuclide.

Radiochemical techniques dealing only with residual nuclei, and not with the emitted particles, are intrinsically not able to discriminate between possible reaction modes or to find out which reaction is really involved; especially in those cases where several reactions producing the same products are energetically feasible. However, in order to evaluate their contributions the following method was used:

Proportional values to the production cross sections "$\sigma_p(\text{mb})\sum_i a_i/\bar{A}$" measured during this work are shown in Table 1 and Figs. 2 to 5.

Threshold energies from KELLER, LANGE and MÜNZEL tables [3] for reactions starting from different stable isotopes are also shown on the respective graphs. From these thresholds it is possible to draw some conclusions as to which reactions are expected to give larger contributions to the lower parts of the curves. After that, the systematic method by LANGE and MÜNZEL [4] was followed.

Absolute cross sections for a given reaction can then be deduced from the curves evaluated in this way and corrected by the ratio between the atomic weight and the isotopic abundance of the target nuclide involved.

Fig. 2 displays $\sigma_p(\text{mb})\sum_i a_i/\bar{A}$ for the production of ^{204}Bi

Table 1

E_d	σ (mb)	σ_p (mb) $\sum_i a_i/\bar{A}$			
(MeV)	^{203}Bi	^{204}Bi	^{205}Bi	^{206}Bi	^{207}Bi
27.32	536.78 ± 188.79	$1.86\times10^{-1}\pm3.82\times10^{-2}$	$1.52\times10^{0}\pm5.84\times10^{-2}$	$1.87\times10^{0}\pm2.48\times10^{-1}$	$2.82\times10^{0}\pm4.34\times10^{-1}$
26.31	565.49 ± 209.44	$7.16\times10^{-2}\pm1.50\times10^{-2}$	$1.55\times10^{0}\pm5.98\times10^{-2}$	$1.68\times10^{0}\pm2.22\times10^{-1}$	$3.22\times10^{0}\pm4.96\times10^{-1}$
25.29	723.33 ± 190.60	$2.14\times10^{-2}\pm5.03\times10^{-3}$	$1.49\times10^{0}\pm5.68\times10^{-2}$	$1.94\times10^{-1}\pm1.32\times10^{-1}$	$3.73\times10^{0}\pm5.75\times10^{-1}$
24.15	731.37 ± 235.00	$1.24\times10^{-2}\pm4.09\times10^{-3}$	$1.34\times10^{0}\pm5.89\times10^{-2}$	$1.73\times10^{-1}\pm1.32\times10^{-1}$	$4.07\times10^{0}\pm6.27\times10^{-1}$
23.05	631.18 ± 181.53	$9.89\times10^{-3}\pm3.15\times10^{-3}$	$1.12\times10^{0}\pm4.30\times10^{-2}$	$1.18\times10^{0}\pm1.56\times10^{-1}$	$3.98\times10^{0}\pm6.12\times10^{-1}$
21.76	436.24 ± 161.55	$1.05\times10^{-2}\pm3.16\times10^{-3}$	$9.78\times10^{-1}\pm3.81\times10^{-2}$	$1.10\times10^{0}\pm1.46\times10^{-1}$	$3.60\times10^{0}\pm5.55\times10^{-1}$
20.46	380.17 ± 140.80	$1.31\times10^{-2}\pm4.25\times10^{-3}$	$7.84\times10^{-1}\pm3.19\times10^{-2}$	$1.06\times10^{0}\pm1.41\times10^{-1}$	$3.32\times10^{0}\pm5.12\times10^{-1}$
19.11	252.20 ± 943.43	$1.91\times10^{-2}\pm4.85\times10^{-3}$	$5.59\times10^{-1}\pm2.33\times10^{-2}$	$1.12\times10^{0}\pm1.49\times10^{-1}$	$3.10\times10^{0}\pm4.78\times10^{-1}$
17.62	458.38 ± 169.75	$1.98\times10^{-2}\pm4.98\times10^{-3}$	$2.24\times10^{-1}\pm1.39\times10^{-2}$	$1.12\times10^{0}\pm1.48\times10^{-1}$	$2.45\times10^{0}\pm3.77\times10^{-1}$
15.98	111.81 ± 147.79	$2.39\times10^{-2}\pm5.60\times10^{-3}$	$3.97\times10^{-2}\pm3.95\times10^{-2}$	$8.10\times10^{-1}\pm1.07\times10^{-1}$	$1.35\times10^{0}\pm2.09\times10^{-1}$
14.21		$1.91\times10^{-2}\pm5.13\times10^{-3}$	$2.20\times10^{-2}\pm1.13\times10^{-2}$	$5.90\times10^{-1}\pm7.80\times10^{-2}$	$8.74\times10^{-1}\pm1.37\times10^{-1}$
12.38		$7.57\times10^{-3}\pm4.29\times10^{-3}$	$4.65\times10^{-3}\pm3.96\times10^{-3}$	$2.98\times10^{-1}\pm3.95\times10^{-2}$	$4.86\times10^{-1}\pm8.49\times10^{-2}$
10.42			$5.38\times10^{-3}\pm1.21\times10^{-2}$	$7.61\times10^{-2}\pm1.01\times10^{-2}$	$1.62\times10^{-1}\pm4.80\times10^{-2}$
7.99			$4.62\times10^{-4}\pm8.42\times10^{-3}$	$1.33\times10^{-3}\pm8.20\times10^{-4}$	$2.94\times10^{-2}\pm2.81\times10^{-2}$
4.80					$2.89\times10^{-2}\pm3.27\times10^{-2}$

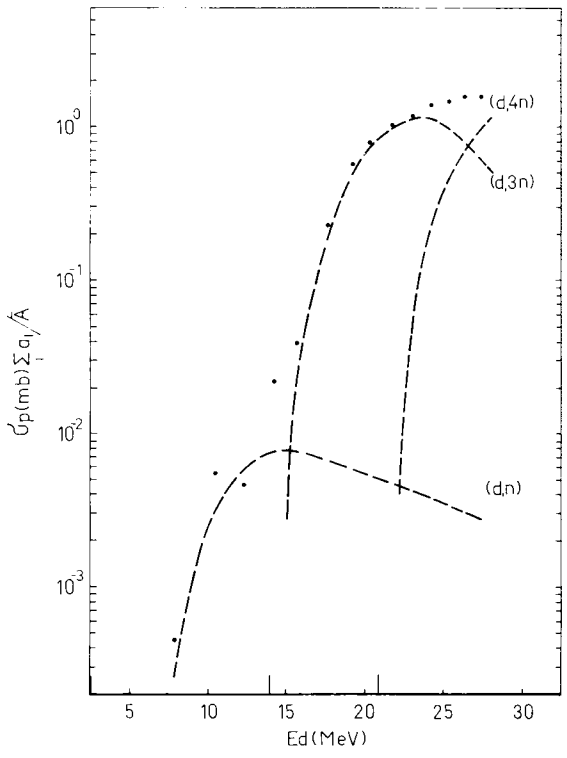

Fig. 3. $\sigma_p(\text{mb})\sum_i a_i/\bar{A}$ for ^{205}Bi. Dashed lines represent the estimates of different possible reactions

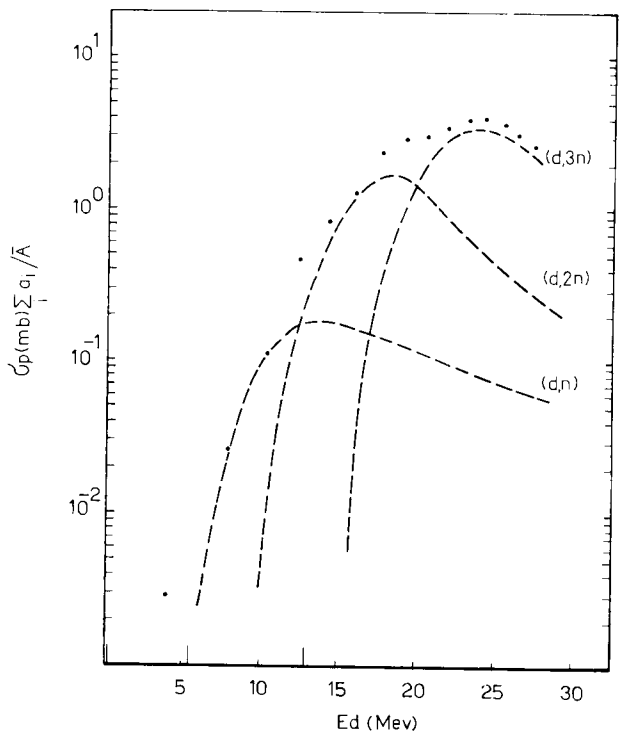

Fig. 5. $\sigma_p(\text{mb})\sum_i a_i/\bar{A}$ for ^{207}Bi. Dashed lines represent the estimates of different possible reactions

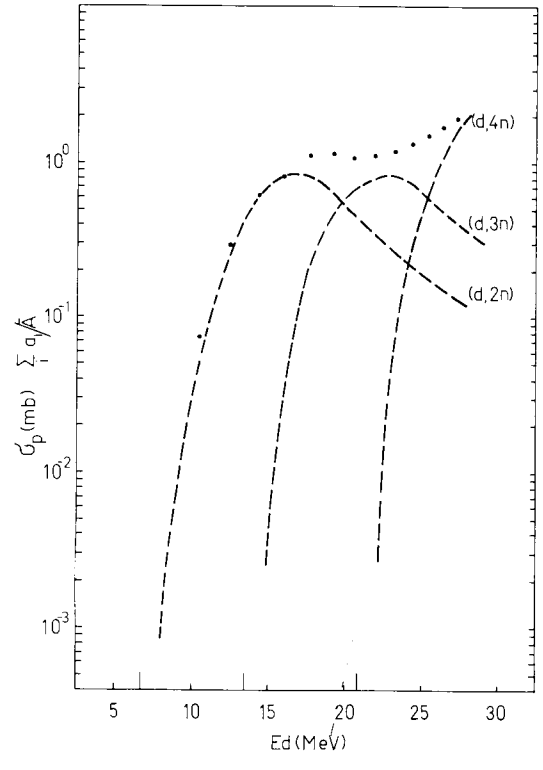

Fig. 4. $\sigma_p(\text{mb})\sum_i a_i/\bar{A}$ for ^{206}Bi. Dashed lines represent the estimates of different possible reactions

as a function of deuteron energy within the depicted energy interval. ^{204}Bi is produced through (d, 2n) and (d, 4n) reactions; dashed curves represent estimates of different possible reactions. No previous determinations of these functions by other authors are known.

Applying our activity values of ^{205}Bi onto $\sigma_p(\text{mb})\sum_i a_i/\bar{A}$ the consequent results were plotted in Fig. 3. Contributions from ^{204}Pn(d, n), ^{206}Pb(d, 3n) and ^{207}Pb(d, 4n) were estimated.

Fig. 4 displays the $\sigma_p(\text{mb})\sum_i a_i/\bar{A}$ for ^{206}Bi produced by ^{206}Pb(d, 2n), ^{207}Pb(d, 3n) and ^{208}Pb(d, 4n) reactions. Dashed lines represent their estimated contributions.

In Fig. 5 the $\sigma_p(\text{mb})\sum_i a_i/\bar{A}$ function for the production of ^{207}Bi is shown. ^{207}Bi is produced through (d, n), (d, 2n) and (d, 3n) reactions; dashed curves represent estimates of different possible reactions.

Absolute cross section values as calculated from our measurements and corrected for isotopic abundance and atomic weight, were compared with those from the systematics of excitation functions [3–4]. Good agreement was found.

The thick target yields for ^{205}Bi, ^{206}Bi and ^{207}Bi production, were calculated through numerical integration, applying experimental cross section values obtained in the present work (Fig. 3, Fig. 4 and Fig. 5), into MÜNZEL and SVOBODA's method [4, 2]. A computer program [21] was developed.

Values for energy integration ranges are listed in Tables 2, 3 and 4. It ought to be kept in mind that for thick

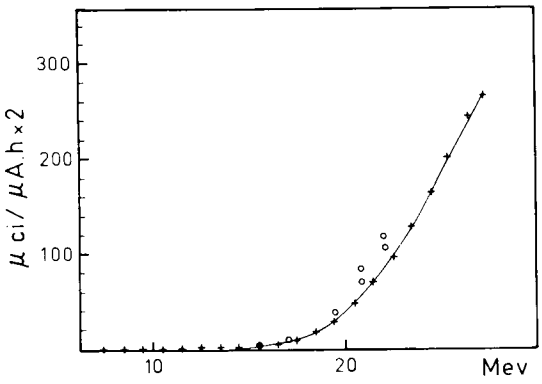

Fig. 6. Thick-target yields for the ^{205}Bi production. ++++ This work, o o o Ref. 22

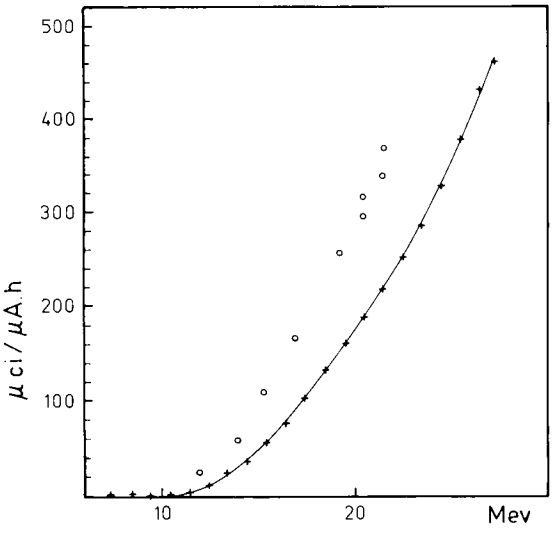

Fig. 7. Thick-target yields for the ^{206}Bi production. ++++ This work, o o o Ref. 22

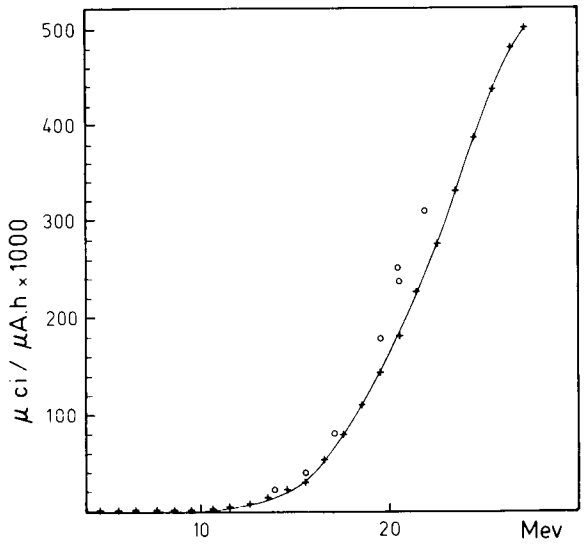

Fig. 8. Thick-target yields for the ^{207}Bi production. ++++ This work, o o o Ref. 22

target results, isotopic abundance was assumed as $\sum_i a_i$ = 0.476, 0.986 and 0.986 respectively. Our results are shown as plots of yields vs. deuteron energy (Fig. 6, Fig. 7 and Fig. 8). P. P. DMITRIEV *et al.* [22], reported on ^{205}Bi, ^{206}Bi and ^{207}Bi yields as related to deuteron energy, when irradiating thick lead metal targets. Comparison with our results shows that the latter values are lower; this may probably be due to the data taken from the excitation functions previously determined in this work.

DMITRIEV *et al.* used a NaI(Tl) crystal as detector; on ^{206}Bi probably the measurement of their activity was affected by the activity of ^{205}Bi having the first gamma rays of 1.71865 MeV (0.34%) and 1.791 keV (0.14%) and the

Table 2

Range Energy (MeV)	Thickness of the target (mg/cm^2)	Production cross section (mb)	Saturation Activity ($\mu C_i/\mu A$)	$\sum$ Saturation Activity ($\mu C_i/\mu A$)	$\sum A_t/10$ ($\mu C_i/\mu A$)	$\sum A_{1h}$ ($\mu C_i/\mu A$h)
27.5 – 27	34.63	1.56	5.495×10^{3}	7.0724×10^{4}	4.736×10^{3}	1.33×10^{2}
27 – 26	69.00	1.60	1.123×10^{4}	6.5229×10^{4}	4.368×10^{3}	1.23×10^{2}
26 – 25	66.00	1.53	1.027×10^{4}	5.3998×10^{4}	3.616×10^{3}	1.02×10^{2}
25 – 24	65.30	1.43	9.499×10^{3}	4.3725×10^{4}	2.928×10^{3}	8.24×10^{1}
24 – 23	63.10	1.26	8.088×10^{3}	3.4225×10^{4}	2.292×10^{3}	6.45×10^{1}
23 – 22	61.20	1.14	7.097×10^{3}	2.6137×10^{4}	1.750×10^{3}	4.92×10^{1}
22 – 21	59.40	1.00	6.042×10^{3}	1.9039×10^{4}	1.275×10^{3}	3.59×10^{1}
21 – 20	57.60	0.84	4.922×10^{3}	1.2996×10^{4}	8.704×10^{2}	2.45×10^{1}
20 – 19	55.70	0.65	3.683×10^{3}	8.0747×10^{3}	5.407×10^{2}	1.52×10^{1}
19 – 18	53.90	0.44	2.412×10^{3}	4.3915×10^{3}	2.941×10^{2}	8.28×10^{0}
18 – 17	51.90	0.22	1.187×10^{3}	1.9788×10^{3}	1.325×10^{2}	3.73×10^{0}
17 – 16	50.00	0.095	4.832×10^{2}	7.9091×10^{2}	5.296×10^{1}	1.49×10^{0}
16 – 15	48.00	0.035	1.709×10^{2}	3.0768×10^{2}	2.060×10^{1}	5.80×10^{-1}
15 – 14	46.00	0.0078	3.650×10^{1}	1.3678×10^{2}	9.159×10^{0}	2.58×10^{-1}
14 – 13	44.10	0.0072	3.185×10^{1}	1.0027×10^{2}	6.715×10^{0}	1.89×10^{-1}
13 – 12	42.00	0.0062	2.649×10^{1}	6.8426×10^{1}	4.582×10^{0}	1.29×10^{-1}
12 – 11	39.90	0.0048	1.948×10^{1}	4.1935×10^{1}	2.808×10^{0}	7.90×10^{-2}
11 – 10	37.90	0.0033	1.272×10^{1}	2.2451×10^{1}	1.503×10^{0}	4.23×10^{-2}
10 – 9	35.70	0.0017	6.355×10^{0}	9.7278×10^{0}	6.514×10^{-1}	1.83×10^{-2}
9 – 8	33.50	0.00084	2.862×10^{0}	3.3722×10^{0}	2.258×10^{-1}	6.35×10^{-3}
8 – 7	31.30	0.00016	5.094×10^{-1}	5.0947×10^{-1}	3.412×10^{-2}	9.60×10^{-4}

Table 3

Range Energy	Thickness of the target	Production cross section	Saturation Activity	$\sum$ Saturation Activity	$\sum A_t/10$	$\sum A_{1h}$
(MeV)	(mg/cm^2)	(mb)	($\mu C_i/\mu A$)	($\mu C_i/\mu A$)	($\mu C_i/\mu A$)	($\mu C_i/\mu Ah$)
27.5 – 27	34.62	1.86	6.552×10^{3}	9.9671×10^{4}	6.675×10^{3}	4.60×10^{2}
27 – 26	69.00	1.72	1.207×10^{4}	9.3119×10^{4}	6.236×10^{3}	4.30×10^{2}
26 – 25	66.00	1.47	9.870×10^{3}	8.1045×10^{4}	5.427×10^{3}	3.74×10^{2}
25 – 24	65.30	1.33	8.835×10^{3}	7.1175×10^{4}	4.766×10^{3}	3.28×10^{2}
24 – 23	63.10	1.23	7.896×10^{3}	6.2340×10^{4}	4.175×10^{3}	2.88×10^{2}
23 – 22	61.20	1.12	6.973×10^{3}	5.4444×10^{4}	3.646×10^{3}	2.51×10^{2}
22 – 21	59.40	1.07	6.465×10^{3}	4.7471×10^{4}	3.179×10^{3}	2.19×10^{2}
21 – 20	57.60	1.05	6.153×10^{3}	4.1005×10^{4}	2.746×10^{3}	1.89×10^{2}
20 – 19	55.70	1.10	6.233×10^{3}	3.4853×10^{4}	2.334×10^{3}	1.61×10^{2}
19 – 18	53.90	1.14	6.251×10^{3}	2.8620×10^{4}	1.917×10^{3}	1.32×10^{2}
18 – 17	51.90	1.04	5.491×10^{3}	2.2369×10^{4}	1.498×10^{3}	1.03×10^{2}
17 – 16	50.00	0.94	4.781×10^{3}	1.6878×10^{4}	1.130×10^{3}	7.79×10^{1}
16 – 15	48.00	0.83	4.053×10^{3}	1.2096×10^{4}	8.100×10^{2}	5.58×10^{1}
15 – 14	46.00	0.68	3.182×10^{3}	8.0432×10^{3}	5.386×10^{2}	3.71×10^{1}
14 – 13	44.10	0.52	2.333×10^{3}	4.8611×10^{3}	3.255×10^{2}	2.24×10^{1}
13 – 12	42.00	0.35	1.495×10^{3}	2.5282×10^{3}	1.693×10^{2}	1.17×10^{1}
12 – 11	39.90	0.16	6.697×10^{2}	1.0327×10^{3}	6.916×10^{1}	4.77×10^{0}
11 – 10	37.90	0.072	2.776×10^{2}	3.6297×10^{2}	2.431×10^{1}	1.67×10^{0}
10 – 9	35.70	0.020	7.264×10	8.5360×10^{1}	5.716×10^{0}	3.94×10^{-1}
9 – 8	33.50	0.0035	1.193×10	1.2724×10^{1}	8.521×10^{-1}	5.87×10^{-2}
8 – 7	31.30	0.00025	7.960×10^{-1}	7.9605×10^{-1}	5.331×10^{-2}	3.67×10^{-3}

Table 4

Range Energy	Thickness of the target	Production cross section	Saturation Activity	$\sum$ Saturation Activity	$\sum A_t/10$	$\sum A_{1h}$
(MeV)	(mg/cm^2)	($\mu C_i/\mu A$)	($\mu C_i/\mu A$)	($\mu C_i/\mu A$)	($\mu C_i/\mu A$)	($\mu C_i/\mu Ah$)
27.5 – 27	34.63	2.65	9.3348×10^{3}	2.396×10^{5}	1.605×10^{4}	4.99×10^{-1}
27 – 26	69.00	2.98	2.0918×10^{4}	2.302×10^{5}	1.542×10^{4}	4.80×10^{-1}
26 – 25	66.00	3.65	2.4507×10^{4}	2.094×10^{5}	1.402×10^{4}	4.37×10^{-1}
25 – 24	65.30	3.95	2.6248×10^{4}	1.848×10^{5}	1.238×10^{4}	3.86×10^{-1}
24 – 23	63.10	4.00	2.5677×10^{4}	1.586×10^{5}	1.062×10^{4}	3.31×10^{-1}
23 – 22	61.20	3.85	2.3970×10^{4}	1.329×10^{5}	8.902×10^{3}	2.77×10^{-1}
22 – 21	59.40	3.50	2.1150×10^{4}	1.089×10^{5}	7.297×10^{3}	2.27×10^{-1}
21 – 10	57.60	3.15	1.8458×10^{4}	8.782×10^{4}	5.881×10^{3}	1.83×10^{-1}
20 – 19	55.70	2.84	1.6093×10^{4}	6.936×10^{4}	4.645×10^{3}	1.45×10^{-1}
19 – 18	53.90	2.78	1.5244×10^{4}	5.327×10^{4}	3.567×10^{3}	1.11×10^{-1}
18 – 17	51.90	2.38	1.2566×10^{4}	3.802×10^{4}	2.547×10^{3}	7.93×10^{-2}
17 – 16	50.00	1.70	8.6472×10^{3}	2.546×10^{4}	1.705×10^{3}	5.31×10^{-2}
16 – 15	48.00	1.19	5.8109×10^{3}	1.681×10^{4}	1.126×10^{3}	3.51×10^{-2}
15 – 14	46.00	0.89	4.1649×10^{3}	1.100×10^{4}	7.366×10^{2}	2.29×10^{-2}
14 – 13	44.10	0.645	2.8937×10^{3}	6.835×10^{3}	4.577×10^{2}	1.43×10^{-2}
13 – 12	42.00	0.430	1.8373×10^{3}	3.942×10^{3}	2.639×10^{2}	8.22×10^{-3}
12 – 11	39.90	0.245	9.9448×10^{2}	2.104×10^{3}	1.409×10^{2}	4.39×10^{-3}
11 – 10	37.90	0.143	5.5135×10^{2}	1.110×10^{3}	7.432×10^{1}	2.31×10^{-3}
10 – 9	35.70	0.086	3.1233×10^{2}	5.585×10^{2}	3.740×10^{1}	1.16×10^{-3}
9 – 8	33.50	0.045	1.5336×10^{2}	2.462×10^{2}	1.648×10^{1}	5.13×10^{-4}
8 – 7	31.30	0.017	5.4131×10^{1}	9.281×10^{1}	6.215×10^{0}	1.94×10^{-4}
7 – 6	29.00	0.0063	1.8586×10^{1}	3.867×10^{1}	2.590×10^{0}	8.07×10^{-5}
6 – 5	26.68	0.0045	1.2214×10^{1}	2.008×10^{1}	1.345×10^{0}	4.19×10^{-5}
5 – 4	24.19	0.0032	7.8748×10^{0}	7.875×10^{0}	5.273×10^{-1}	1.04×10^{-5}

later of 1.76427 MeV (27%) and 1.7758 keV (2.8%). On ^{207}Bi they used the 570 keV gamma ray; the ^{205}Bi has also peaks of 561.2 keV (0.05%), 570.58 keV (4.5%), 573.7 keV (0.5%), 576.3 keV (0.3%) and 579.78 keV (4.8%) that could affect the activity of ^{207}Bi if the decay time was not large enough. We used the 1063.62 keV ray measured with a solid state detector.

Acknowledgment

The authors are indebted to the Synchrocyclotron staff who performed the irradiations.

References

1. SVOBODA, K., SILVESTER, D. J.: Quantities and Units Used in the Production of Radionuclides by Charged Particle Bombardment. Int. J. Appl. Radiat. Isot. 23, 203 (1972).
2. SVOBODA, K.: On Terms Used in the Production of Radioisotopes by Charged Particle Bombardment. Ú. J. V. Report 2258 Ch. Czechoslovakia (1969).
3. KELLER, K. A., LANGE, J., MÜNZEL, H., PFENNIG, G.: Landolt-Börnstein Numerical Data and Functional Relationships in Science and Technology, I Vol. 5, part a (1973), b (1973), and c (1974).
4. LANGE, J., MÜNZEL, H.: Abschätzung Unbekannter Anregungsfunktionen für (α, xn), (α, pxn), (d, xn), (d, pxn) und (p, xn) Reaktionen. KFK-767 (1968).
5. CHACKETT, G. A., CHACKETT, K. F., WELBORN, J. B.: The preparation of Carrier-Free ^{203}Pb For Medical Use. Int. J. Appl. Radiat. Isot. 22, 715 (1971).
6. STARK, V. J., HARPER, P. V., LATHROP, K. A., KRIZEK, H., ROWED, D. W., LEMBARES, N., HOEFER, P. B.: Evaluation of ^{203}Pb as an Imaging Agent for Cisternography. J. Nucl. Med. 13, N° 6, 468 (1972).
7. QAIM, S. M., WEINREICH, R., OLLIG, H.: Production of ^{201}Tl and ^{203}Pb via Proton Induced Nuclear Reactions on Natural Thallium. Int. J. Appl. Radiat. Isot. 30, 85 (1979).
8. SILVESTER, D. J.: Accelerator Production of Medically-Useful Radionuclides. Radiopharmaceuticals and Labelled Compounds; IAEA – SM – 171/6 Proceedings of a Symposium Copenhagen, 26 – 30 March 1973. Organized by the IAEA and WHO, Vol. 1, p. 197.
9. BETANCOURT, I. DE; NASSIFF, S. J.: Excitation Functions for Deuteron Induced Reactions on Tantalum. Radiochim. Acta 12, 206 (1969).
10. SIRI, L. N., NASSIFF, S. J.: Excitation Functions for ^{159}Tb (d, p) ^{160}Tb and ^{159}Tb (d, 4n) ^{157}Dy Reactions. Radiochim. Acta 14, 159 (1970).
11. NASSIFF, S. J., MÜNZEL, H.: Excitation Functions for Deuteron Induced Reactions on Zinc. Radiochem. Radioanal. Lett. 12, 6, 353 – 361 (1972).
12. NASSIFF, S. J., MÜNZEL, H.: Cross Sections for the Reactions ^{66}Zn (d, n)^{67}Ga, ^{52}Cr (d, 2n) ^{52g}Mn and ^{186}W (d, 2n) ^{186}Re. Radiochim. Acta 19, 97 (1973).
13. LALLI, M. E., WASILEVSKY, C., HERREROS, O. R., NASSIFF, S. J.: Excitation Functions and Isomeric Ratios for the Isomeric Pair ^{106m}Ag and ^{106g}Ag in the ^{107}Ag (d, t) Reaction. Radiochim. Acta 23, 107 (1976).
14. MARTENS, U., SCHWEIMER, G. W.: Production of ^{7}Be, ^{22}Na, ^{24}Na and ^{28}Mg by Irradiation of ^{27}Al with 52 MeV Deuterons and 104 MeV Alpha Particles. Z. Physik 233, 170 (1970) or KFK 1083.
15. WILLIAMSON, C. F., BOUJOT, J. P., PICARD, J.: Tables of Range and Stopping Power of Chemical Elements for Charged Particles of Energy 0.05 to 500 MeV Report CEA-R-3042 (1966).
16. SELTZER, S. M., BERGER, M. J.: Energy Loss Straggling of Protons and Mesons: Tabulation of the Vavilov Distribution, NAS-NRC-PUB-1133, 187 – 203 (1964).
17. BAEDECKER, P. A.: Digital Methods of Photopeak Integration in Activation Analysis. Anal. Chem. 43, 409 (1971).
18. TACZANOWSKY, S.: Precision of Direct Methods of Photopeak Integration in Cases of Sloping Background. I. T. J. N° 37/I (1973).
19. Nuclear Data Sheets. Vol. 5, 5; Vol. 5, 6; Vol. 23, 2; Vol. 7, 2; Vol. 22, 4.
20. ERDTMANN, G., SOYKA, W.: Die Gamma-Linien der Radionuclide JÜL-1003-AC (1973).
21. Unpublished. Dicke: A computer program for Thick Target Yields.
22. DMITRIEV, P. P., KRASNOV, N. N., MOLIN, G. A., PANARIN, M. V.: Yields of ^{205}Bi, ^{206}Bi and ^{207}Bi from Lead irradiated with protons or deuterons, UDC 539.172.12. Translated from At. Energ. 33, N° 4, 976 (1974).